

Development and Application of Multidisciplinary Coupled Computational Techniques for Projectile Aerodynamics

J. Sahu^{*}, M. Costello^{**} and C. Montalvo^{**}
Corresponding author: jubaraj.sahu.civ@mail.mil

^{*} U. S. Army Research Laboratory, APG, MD, USA
^{**} Georgia Institute of Technology, Atlanta, GA, USA.

Abstract: The present work is focused on the development and application of advanced state-of-the-art time-accurate coupled computational fluid dynamics (CFD)/rigid body dynamics (RBD)/flight control system (FCS) techniques for prediction of the unsteady free-flight aerodynamics and flight behavior of projectiles in an integrated manner. The added element of this coupling is the FCS or the guidance, navigation, and control aspect. An interface was created and developed for easy transfer of both the RBD state variables and the flight control system variables of interest between the CFD flow solver and RBD/FCS code. The coupled CFD/RBD/FCS capability has been exercised on a canard-controlled projectile and has been demonstrated using a guided roll control and a guided cross-range control example. Coupled results obtained show the resulting canard deflection angles and their effect on the aerodynamics and flight dynamics of this projectile during the guided maneuvers.

Keywords: Computational Fluid Dynamics, Multidisciplinary Coupled Methods, Projectile Control, Time-accurate Virtual Fly-Out.

1 Introduction

Accurate determination of aerodynamics and flight dynamics is critical to the low-cost development of new affordable munitions. Recent advances made in high performance computing (HPC) and computational fluid dynamics (CFD) technologies have the potential for greatly reducing the design costs while providing a more detailed understanding of the complex aerodynamics than the understanding achieved through experiments and actual test firings. Three-dimensional (3-D) steady and unsteady Navier-Stokes computational techniques have been used to predict aerodynamics of both spinning and fin-stabilized projectiles from subsonic to supersonic speeds [1-2]. Both steady-state and time-accurate CFD techniques are routinely used. Time-accurate or unsteady CFD modeling techniques have proven more challenging but are increasingly being used for numerical prediction of unsteady projectile and missile aerodynamics [3-9]. In particular, time-accurate methods are used for dynamic derivatives such as the Magnus moment and pitch-damping moment of projectiles. Accurate determination of dynamic derivatives is critical as they influence the dynamic stability of the projectiles. Fully time-accurate methods offer the greatest potential of providing accurate prediction of these dynamic derivatives. Algorithm and computing advances have also led to coupling of CFD codes to rigid body dynamics (RBD) codes for the simulation of projectile free flight motion in a time accurate manner [10].

As part of a Department of Defense HPC grand challenge project, the U.S. Army Research Laboratory (ARL) has recently focused on the development and application of state-of-the-art coupled CFD and RBD algorithms for prediction of unsteady aerodynamics and flight dynamics of projectiles with and without flow control maneuvers [7, 9]. Our objective is to exploit advanced CFD techniques and coupled methods on HPC platforms for design and analysis of unguided and guided projectiles. For maneuvering munitions, the effect of many weapon control mechanisms, such as canards, deployable pins, pulsed flaps, and microjets on flight dynamics is critical to guided flight performance. Many of these mechanisms fall outside the range of conventional aerodynamic control and accurate well-validated tools for prediction of aerodynamic loads are desired. These control mechanisms result in highly complex, unsteady flow interactions and their accurate modeling during guided flight with active control is a major challenge. Knowledge of the detailed unsteady aerodynamics of maneuvering precision weapons is rather limited. Multidisciplinary computations has the potential to provide detailed fluid dynamic understanding of the unsteady aerodynamics processes involving the maneuvering flight of modern guided weapon systems. Such knowledge cannot be obtained easily by any other means. A lot of progress has been made recently with the computational technology involving CFD and RBD for prediction of unsteady aerodynamics and flight dynamics of projectiles without control maneuvers [2, 10]. For simulation of control maneuvers, a flight control system (FCS) has now been integrated into the coupled CFD/RBD procedure. The resulting CFD/RBD/FCS coupled capability can now be exploited to determine the unsteady aerodynamics and flight dynamics associated with conventional and new aerodynamic control technologies for maneuvering precision munitions.

Coupled CFD/RBD virtual fly-out technique has already been demonstrated and validated a finned projectile at a supersonic speed, [10] a spinning projectile at subsonic speed [7], and another spinning projectile at transonic speeds [2]. Validation of the computed results from the virtual fly-out simulations was accomplished with comparison to free flight test data. Ongoing research and coupling of FCS with CFD/RBD procedure now is beginning to extend the capability of the coupled technique further for simulation of control maneuvers. BoomFCS [11] has been integrated to provide that added FCS capability. This code has the flight control design capability that allows us to compute the unsteady aerodynamics and flight dynamics associated with guided maneuvers. The advanced CFD capability used in the coupled CFD/RBD/FCS procedure solves the Navier-Stokes equations, incorporates unsteady boundary conditions, special coupling procedure, and restart capability.

This paper describes the progress made in the development and application of the coupled CFD/RBD/FCS methods to projectile aerodynamics. The following sections describe the solution technique, coupled CFD/RBD/FCS procedures and the computed results obtained for guided maneuvers on a canard-controlled finned projectile.

2 Computational Methodology

2.1 CFD Technique

The complete set of three-dimensional (3 D) time-dependent Reynolds-Averaged Navier-Stokes (RANS) equations [12] is solved in a time-accurate manner for simulations of unsteady flow fields associated with both spin-stabilized and finned projectiles during flight. The 3-D time-dependent RANS equations are solved using the finite volume method [13-14]:

$$\frac{\partial}{\partial t} \int_V \mathbf{W} dV + \oint [\mathbf{F} - \mathbf{G}] \cdot d\mathbf{A} = \int_V \mathbf{H} dV \quad (1)$$

where \mathbf{W} is the vector of conservative variables, \mathbf{F} and \mathbf{G} are the inviscid and viscous flux vectors, re-

spectively, \mathbf{H} is the vector of source terms, V is the cell volume, and A is the surface area of the cell face. Second-order discretization was used for the flow variables and the turbulent viscosity equations. Two-equation $k-\varepsilon$ [15] turbulence models were used for the computation of turbulent flows. Dual time-stepping was used to achieve the desired time-accuracy.

2.2 Coupled CFD/RBD/FCS Procedure

For cases with no guided maneuvers, the coupled CFD/RBD technique allows physics-based virtual fly-out simulations of munitions similar to what happens in free flight. As shown in Figure 1, the RBD or the six degrees of freedom (6 DOF) comprises of the inertial position components of the projectile mass center (x, y, z) and the three standard Euler angles (ϕ, θ, ψ), roll angle, pitch angle, and yaw angle, respectively.

For simulations of guided control maneuvers, a coupled CFD/RBD/FCS procedure has been developed by integrating FCS into the coupled CFD/RBD method. The added element of this coupling is the guidance, navigation, and control aspect. An interface was created and developed for easy transfer of both the RBD state variables and the flight control system variables of interest between the CFD flow solver and RBD/FCS code. The BoomFCS [11] code which was specifically designed to predict the atmospheric flight mechanics of smart weapon systems readily provides the needed FCS. In BoomFCS [11], control of a projectile can be achieved in many different ways, e.g., with canards and pulse jets during the flight. Not only are many different control mechanisms used to control projectiles, many different strategies are employed to guide and control a projectile. The control system strategy is conveyed through the control law. The control law stipulates a set of operations that are performed on sensor data to determine how the controls should be changed in flight.

In the coupled CFD/RBD/FCS procedure, the aerodynamic forces and moments are computed at every time step in the CFD solver and transferred to BoomFCS which does both RBD and FCS calculations. The FCS calculation provides as output the flight control variables based on a given FCS design. The FCS design allows for modeling of both controlled and prescribed motions. The output of RBD state and the control variables are transferred to the CFD flow solver which then computes the aerodynamic forces and moments subject to these RBD state and control variables. For example, for a canard-controlled projectile, the output of the FCS variables would be the canard deflection angles. As canards are deflected with the FCS generated deflection angles, the flow solver must take into account the canard motion. Similarly, a set of different FCS variables could be used for a jet-controlled maneuver. As this FCS coupling matures, additional control variables will be used for a variety of controlled flights.

In the present work, canards are used as the control maneuver mechanisms (see Figure 2). The canards are deflected to generate control forces required to maneuver the projectile in roll, pitch, or a combination of both. As shown in figure 1, the projectile in this study is fit with two canards at the nose of the projectile. These canards are dithered such that a normal force is produced. As the projectile rolls the canards can be dithered in an oscillatory fashion to always push the projectile in one direction. For this work a simple cross range controller is developed merely to show the match between the 6DOF and CFD models. Thus the y -coordinate of the projectile is commanded to 2m. As the control algorithm is not the primary basis of this research a simple proportional-derivative-integral (PID) controller is used.

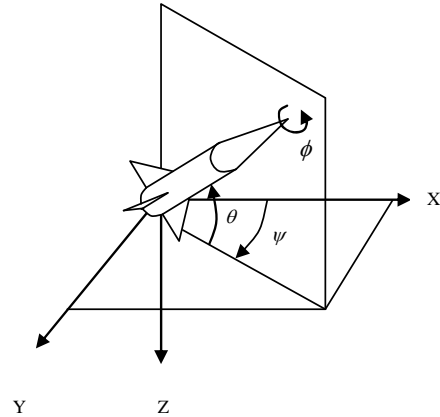


Figure 1. 6-DOF Schematic.

The canard deflection angle is then given by the equation below.

$$\delta_c = \sin(\phi) (K_P(y - y_c) + K_D\dot{y} + K_I \int (y - y_c)dt)$$

The gains K_P , K_D , and K_I are chosen experimentally to obtain a desirable time response of the system. The ‘sin’ component is present so that the canards are only fully actuated when the z-axis of the projectile is parallel to the y-axis of the inertial frame. This also takes care of the direction depending on which direction the z-axis is pointing. As there are two canards this command is sent to each canard such that no roll moment is produced and only a normal force.

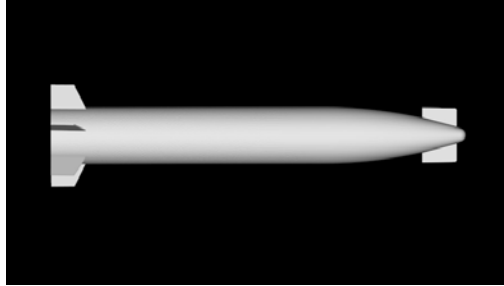


Figure 2: Canard-controlled finned projectile geometry.

To test a variety of different control maneuvers another control system is used to command the Euler roll angle of the projectile to a desired angle. Again since the control system is not the focus of this study a simple proportional derivative controller is used.

$$\delta_c = K_P(\phi - \phi_c) + K_D\dot{\phi}$$

Again the gains are chosen to obtain a desirable time response. No integral gain is needed in this control system as the system does not contain any steady state error in roll. In this system the canards are sent equal and opposite commands so that a pure roll moment is produced and no normal force.

The projectile state vector is comprised of the inertial position components of the projectile mass center (x, y, z) , the standard Euler angles (ϕ, θ, ψ) , the body frame components of the projectile mass center velocity (u, v, w) , and the body frame components of the projectile angular velocity vector (p, q, r) . The entire state vector consisting of these twelve variables is required in the initial conditions before a virtual fly-out can be performed and coupled dynamic solution can be obtained. Typically, we begin with a computation performed in “steady-state mode” with the grid velocities prescribed to account only for the translational motion component of the complete set of initial conditions to be prescribed. At this stage, we also impose the angular orientations from the initial conditions and spin rate is added. Computations are performed with the spin in a time-accurate mode for a desired number of spin cycles. Converged solution from this step provides the initial condition for the next step where a completely coupled CFD/RBD/FCS computation is performed in time-accurate mode. Here, a complete set of initial conditions includes all translational and rotational velocity components and accounts for initial position and angular orientations. In addition, FCS is activated at the beginning of this coupled run for physics-based guided virtual fly-out simulations of munitions.

3 Computational Model and Meshes

Of interest here is the control of projectile using canards as the maneuver or control mechanism. The canards are deflected to generate control forces required to maneuver the projectile in roll, pitch, or a combination of both. The canard-controlled projectile considered in this study has two canards and six fins (see Figure 2). The control maneuver is achieved by two canards located in the nose section of the projectile. All six fins are located at the aft end of the projectile. An unstructured grid is generated for the projectile body with the fins which forms the background mesh (See Figure 3). In general, most of the grid points are clustered in the boundary-layer, nose canards, afterbody fins, and the wake regions. The boundary layer spacing near the wall was selected in order to achieve a y^+ value of 1.0. The unstructured mesh was generated using the Multipurpose Intelligent Meshing Environment (MIME) grid-generation software recently developed by Metacomp Technologies [16]. Clustering of grid points in the regions near the wake, fins, and the canards was achieved using density boxes in MIME. Unstructured grids are also generated about each canard separately (see Figure 4) using the same software. The two canard grids are then overset with the background projectile mesh to a Chimera [17] overlapped mesh for the canard-controlled projectile. The total number of grid points in this case is approximately 12 million. This Chimera procedure requires proper transfer of information between the background mesh and the canard meshes. However, the advantage is that the individual grids are generated only once and the Chimera procedure can then be applied repeatedly as required during the canard motion. There is no need to generate meshes at each time step during the canard maneuvers.

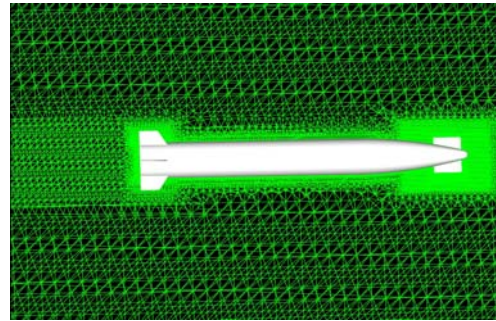


Figure 3. Unstructured mesh near the body.

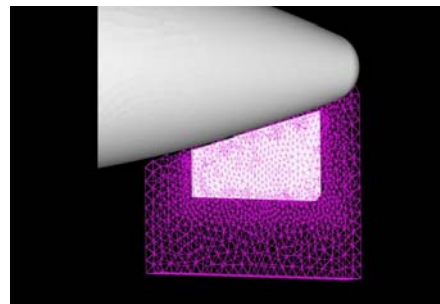
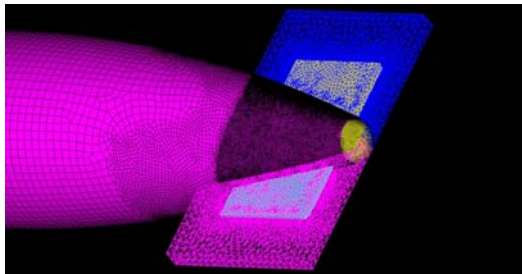


Figure 4: Unstructured Chimera meshes in the nose region of the projectile.

4 Results

Physics-based virtual fly-out computations have been performed for the canard-controlled finned projectile using the coupled CFD/RBD/FCS procedure described above. Full three-dimensional time-accurate solutions have been obtained and no symmetry was used. Demonstration of the coupled CFD/RBD/FCS technique has been achieved using a roll control maneuver and a cross range control maneuver.

Appropriate FCS designs or controllers have been developed for use in the coupled CFD/RBD/FCS calculations for both of these cases. A simple proportional derivative control law is

used for roll control and a PID controller is used for the feedback loop in the cross-range controller. In each of these two cases, the projectile initially is a straight level flight and the initial spin rate is set to zero. Also, the maximum canard deflection angle was prescribed. The first step in the coupled virtual fly-out simulations is the generation of a steady-state solution for the projectile moving forward at a velocity ($M = 0.9$) at zero degree angle of attack. Time-accurate calculations are performed for a few hundred time steps in an uncoupled mode. A solution obtained in the uncoupled mode serves as the starting solution for the fully coupled CFD/RBD/FCS run. The coupled run starts to deflect the canards in accordance with the control law in the FCS design or the controller. The canard deflections are passed onto the CFD solver where the canards are actuated accordingly and CFD results are obtained in a time-accurate manner. CFD predicted aerodynamic forces and moments are then transferred to the RBD/FCS code and new RBD state variables and FCS variables (canard deflections) are computed. Computed coupled results obtained for both the roll and cross control maneuvers are presented next.

4.1 Roll Control Maneuver

A first test case considered is the pure roll control of the canard-controlled finned projectile. The rear fins in this case have no fin cant. For this roll control case, canards on each side are deflected in opposite directions (see Figure 5) and the projectile starts to roll. In this case, a FCS design, i.e., a roll controller was developed and used to command the projectile to a desired roll angle of 5° . The maximum canard deflection angle was first set to 5° . Deflecting the canards in opposite directions gives rise to a differential force and thus a rolling moment for the projectile to roll clockwise (looking forward from the back of the projectile). The canard deflection produces positive or negative force depending on the sign of the canard deflection angle. The movement of the canards affects not only the flow locally in the nose region, but also, the flow field downstream near the aft body with the fins. Figure 6(a) shows the particle traces emanating from one of the canards and as shown in this figure, these particle traces pass through the region in between the two rear fins without affecting the flow near the fins. On the other hand, with the canard deflected (see Figure 6b) the canard particle traces clearly affect the flow on one of the rear fins. This interference effect of the canard on the rear fin can be significant and is taken into account in the coupled CFD/RBD/FCS calculations. Figure 7 shows the computed surface contours on a rear fin being affected by the canard deflection. The top view and bottom view show the surface pressures on the top and bottom fin surfaces, respectively. As shown in Figure 5a, when the canard deflection angle is near zero, the pressures on the top and the bottom surfaces are nearly identical producing no force on this rear fin. However, with the canards deflected the pressures change considerably with higher pressures on the top surface and lower pressures on the bottom fin surface. In this case, the interference effect of the canards on the rear fins leads to a counter clock-wise roll moment. It is an adverse effect and negates the desired roll moment in the clockwise direction.

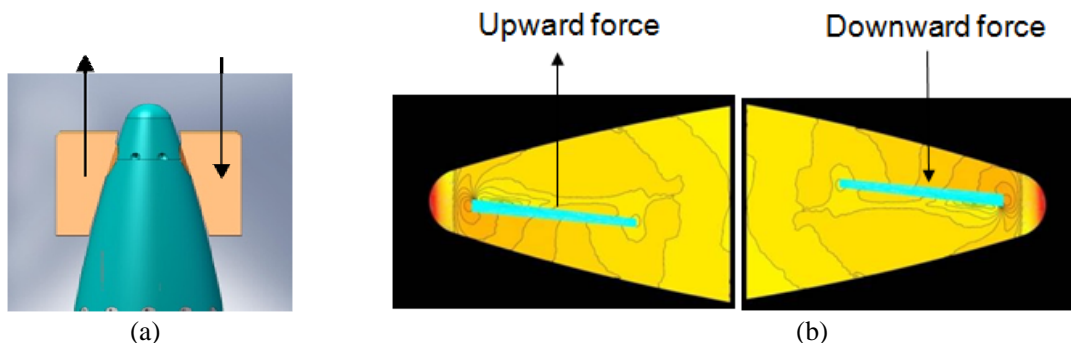


Figure 5. Canards in the nose region, (a) top view (b) side views of left and right canards.

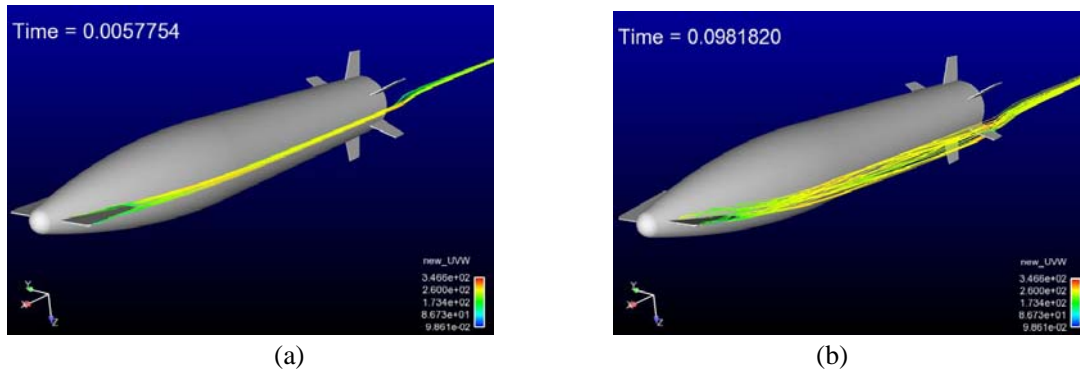


Figure 6. Effect of canard particle traces on rear fins, $M = 0.9$, $\alpha = 0^\circ$ (a) canard undeflected (b) canard deflected.

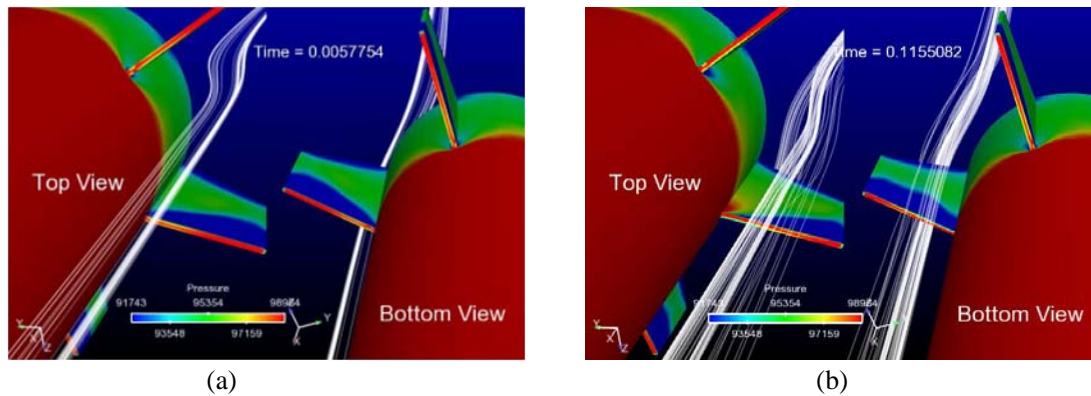


Figure 7. Computed surface pressure contours on a rear fin, $M = 0.9$, $\alpha = 0^\circ$ (a) canard undeflected (b) canard deflected.

Figures 8(a) and 8(b) show the time histories of the roll angle and the roll moment of the projectile, respectively. A computed result from the coupled CFD/RBD/FCS calculation is shown in red and is compared with the results obtained using a standard control design method (BoomFCS) shown in blue. In the standard control design method, the baseline aerodynamics used for the projectile with canards in the undeflected position was generated [18] from a virtual fly-out computation. The aerodynamic model for the deflecting canards came from lifting line theory. As shown in Figure 8(a), initially the roll angle is zero, starts to increase and reaches the commanded value, 5° quickly (in about 0.2 sec) in the standard control simulation. However, the coupled CFD/RBD/FCS calculation predicts a much slower response and reaches the commanded roll angle in about 0.8 sec. Figure 8(b) shows the roll moment of the projectile used in both methods. As seen here, the roll moment predicted in the coupled method using CFD is generally much smaller in magnitude compared to that used in the standard control design method. Unlike the standard control method, the coupled method takes into account the aerodynamic interference effects of the canards on the downstream on the body including the fins. Although the canard deflections produce a positive roll, the interference effect on the rear fins adversely results in a negative roll moment contribution. The total roll moment in the coupled calculation is, thus, not as large as that used in the standard control method which does not include this interference effect.

Figure 9 shows the spin rate as a function of time. Results obtained from both methods are compared to each other. Again, the time responses are quite different. Initially, both methods show

the spin rate to increase to about 0.1 and match well. In the coupled method it then remains constant until $t = 0.6$ s and gradually drops to zero with increasing time. The standard method shows a big rise in the spin rate to 1.1 which is consistent with the larger rolling moment used. Figure 10 shows the actual deflection of one of the canards used in the coupled CFD/RBD/FCS method. With the FCS on, the canard starts deflecting and reaches -5° , its minimum, very quickly and stays constant at that value for a while until $t = 0.55$ s and reaches almost zero towards the end of the simulation. These results correspond to one FCS control design. The maximum canard deflection angle and control law parameters can be adjusted and are varied to next to see their effect on the roll control characteristics.

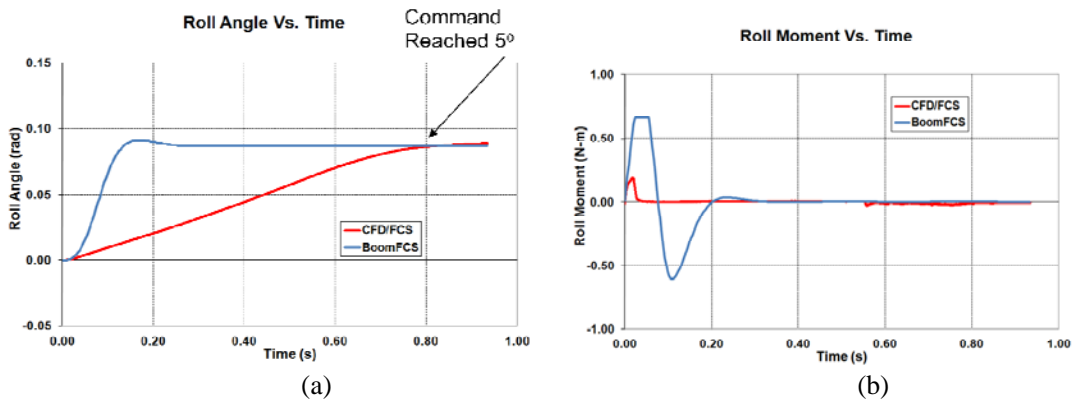


Figure 8. Roll angle (left) and roll moment (right) as a function of time.

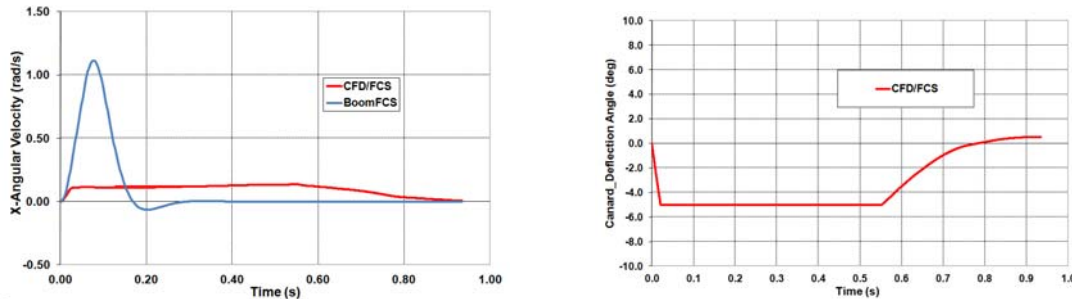


Figure 9. Spin rate vs. time.

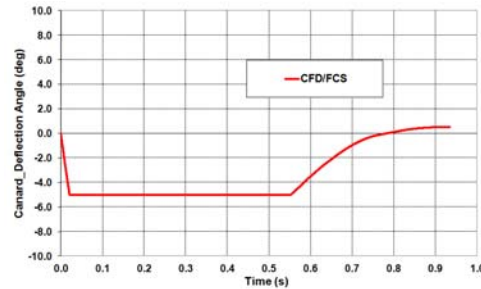


Figure 10. Canard deflection angle vs. time.

CFD/RBD/FCS computed results were also obtained with the maximum canard deflection angle set to 10° . For this case, the effect of FCS parameters (proportional gain, K_p and derivative gain, K_D) were also investigated. Figure 11 shows the roll angle and the roll moment as a function of time. The best response is obtained for $K_p = 5.0$ and $K_D = 0.2$. In this case, as shown in Figure 11a, the roll angle reaches its commanded value of 5° in 0.6 seconds. Varying the derivative gain seems to have little impact on the results. However, when the proportional gain, K_p was reduced from 5.0 to 0.5, the response is a lot slower and hence is not desirable. The corresponding roll moment variation with time is shown in Figure 11b and the corresponding spin rate and the canard deflection angle variations with time are shown in Figures 12 and 13, respectively. As seen in Figure 11b, the roll moment is seen to increase initially, reaches its peak, and then drops to almost zero. This initial rise in the roll moment is due to canards being deflected (see Figure 13). At the same time, the spin rate (see Figure 12) is seen to increase. The roll moment drops to very small (almost zero) values when the canards stop moving (approximately at $t = 0.05$ s for cases with K_p of 5.0) and changes very little with time until the canards moving again around 0.2 sec in time. For the case with $K_p = 5.0$, the net roll moment is negative as the canard deflection angle goes back to close zero. Correspondingly, the spin

rate is found to decrease when $K_p = 5.0$. Computed results show similar behavior in the variation of spin rate and also in the canard deflection angles for both cases with $K_p = 5.0$. A slower response and a slightly different behavior are seen with a smaller value K_p of 0.5. Because of the slower response, computations were stopped after 0.55 sec in time and were not continued further.

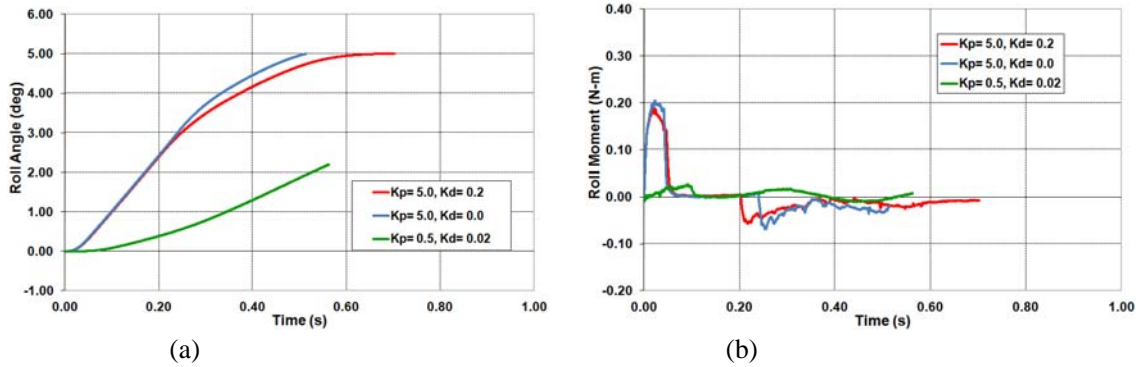


Figure 11. Roll angle (left) and roll moment (right) as a function of time, maximum canard deflection angle = 10° .

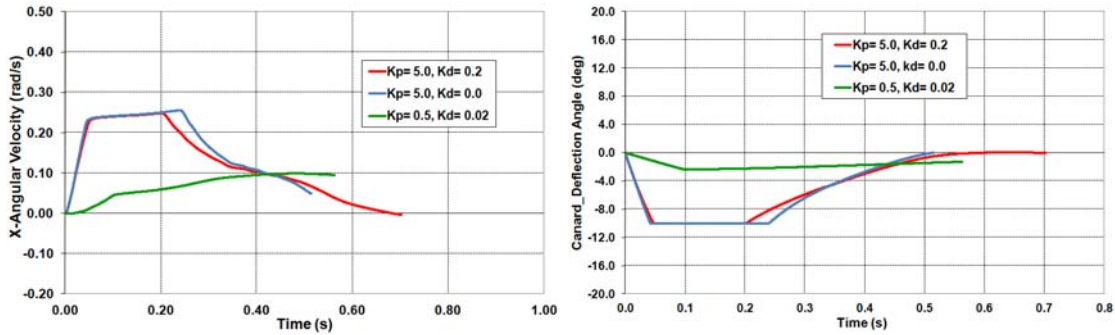


Figure 12. Spin rate vs. time, maximum canard deflection angle = 10° .

Figure 13. Canard deflection angle vs. time, maximum canard deflection angle = 10° .

Figures 14, 15, and 16 show the comparisons of computed responses obtained from the coupled CFD/RBD/FCS solutions with the maximum canard deflection angle set to 5° and 10° . As seen in Figure 14a, the results show that a better response for the roll angle is achieved with maximum canard deflection angle set at 10° . In this case, the commanded roll angle is achieved in 0.6s compared to 0.8s with the maximum canard deflection angle set to 5° . Figure 14b shows similar behavior in the roll moment variation with time. In both cases, the roll moment reaches the same peak value (0.18 N-m) initially. It then drops to almost zero at $t=0.025s$ and $0.05s$ and then later becomes negative at $t=0.55s$ and $0.2s$ for the cases with maximum canard deflection 5° and 10° , respectively. The corresponding spin rate and canard deflection angle variations with time are shown, respectively in Figures 15 and 16. The spin rate variations (Figure 15) show similar behavior for both cases. In both case, the spin rate rises initially until it reaches a peak as canards are deflected (see Figure 16) and roll moment is produced (Figure 14b). The spin rate then is seen to increase very slowly because of a positive but a very small roll moment and subsequently, it then decreases and approaches zero because of the negative roll moment with the canards moving back to zero deflection angle.

Computed results presented above (see Figures 8 and 11) show the time dependent responses on the roll control with a better response obtained when the maximum canard deflection angle was set to 10° . These results also clearly show the adverse interaction effect of the canards on the rear fins in a

direction opposite to the desired roll. The coupled results which take into account this adverse effect indicate that it is perhaps not possible to obtain a much faster response of roll control needed in practical applications with the front two canards. It is possible that there is a maximum canard deflection angle that can be used to decrease the amount of rear fin interaction. This will require further investigation into the roll control problem.

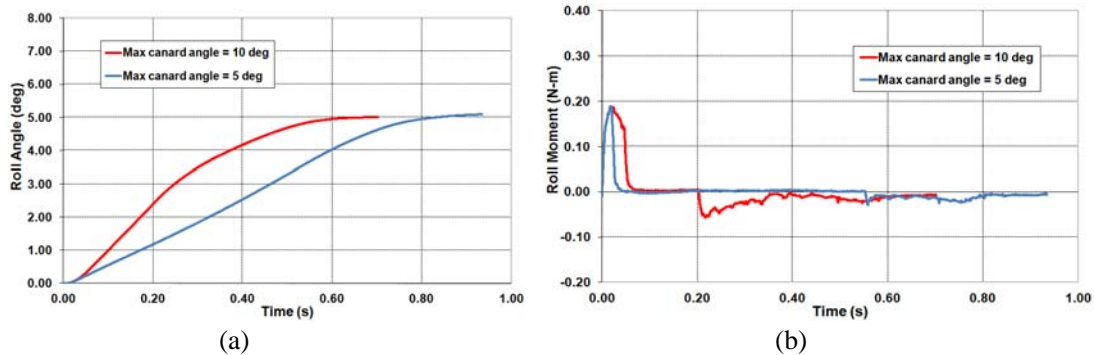


Figure 14. Roll angle (left) and roll moment (right) as a function of time.

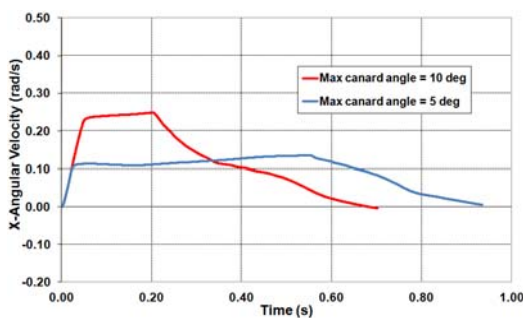


Figure 15. Spin rate vs. time.

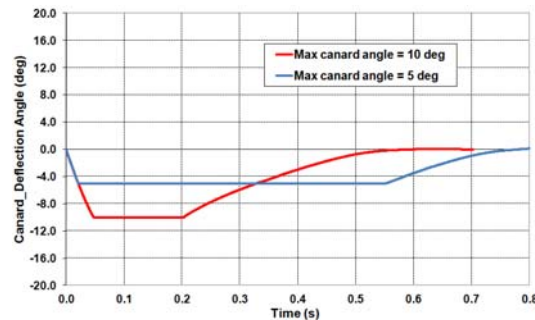


Figure 16. Canard deflection angle vs. time.

4.2 Cross-Range Control Maneuver

Another case considered is the cross-range control of the same canard-controlled finned projectile. The rear fins had a small cant of about 1.25° to produce roll as the projectile flies forward. In this case with the cross-range control, canards on each side are deflected in the same direction as the projectile starts to spin and move forward. Here, a FCS design i.e. a cross-range controller was first developed and used to command the projectile to a desired cross-range (y) of 2m (see Figure 17).

Coupled CFD/RBD/FCS calculations were performed with the FCS design where the proportional and derivative gain parameters were both set to 0.1. Figure 18a and Figure 18b, respectively show the cross-range distance and the canard deflection angle obtained using the coupled CFD/RBD/FCS simulation. Figure 18a shows the cross-range (y) as a function of time. As seen in this figure, it takes a little less than two seconds to reach the commanded cross-range value of 2 m. Although we are able to guide the projectile to its commanded value, the response seems to be oscillatory in nature and is perhaps not desirable. The corresponding canard deflections used in the coupled calculation is shown in Figure 18b. Initially, the canard deflections are smooth up to 0.6s. Later in time one can notice that the canard deflection reaches the maximum ($+10^\circ$) and minimum (-10°) which indicate that the controller is saturated. Figures 19a and 19b show the variation of computed aerodynamic forces and moments with time for this case. These figures clearly show the unsteady nature of the aerodynamic

forces and moments during the flight. As seen in Figure 19a, the amplitudes of oscillations is seen to increase with time indicating an increase in the aerodynamic angle of attack. Similar behavior, although not as pronounced, is also observed in the aerodynamic moment components (see Figure 19b).

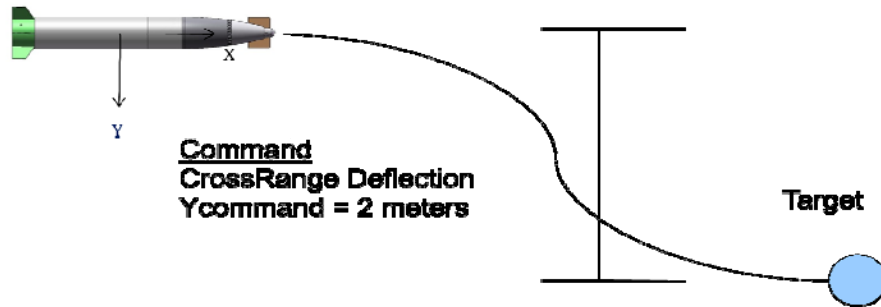


Figure 17. Schematics of guided cross-range control maneuver.

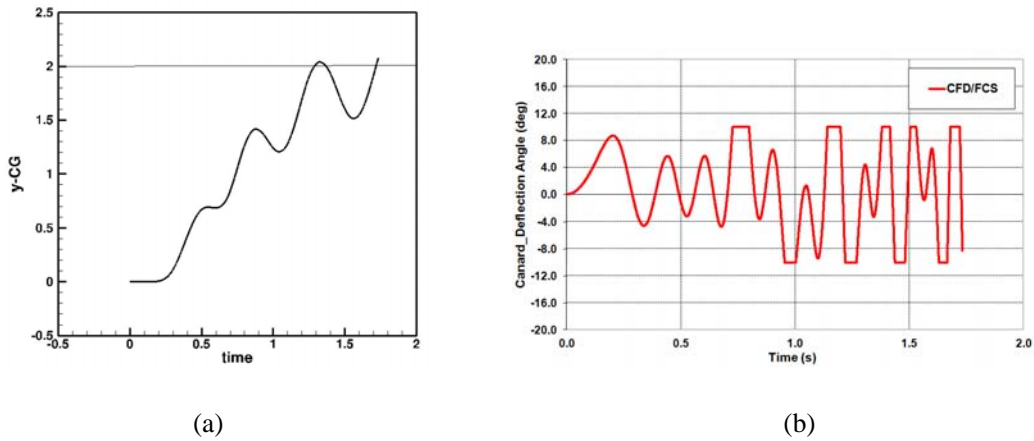


Figure 18. Cross-range distance (left) and Canard deflection angle (right) as a function of time.

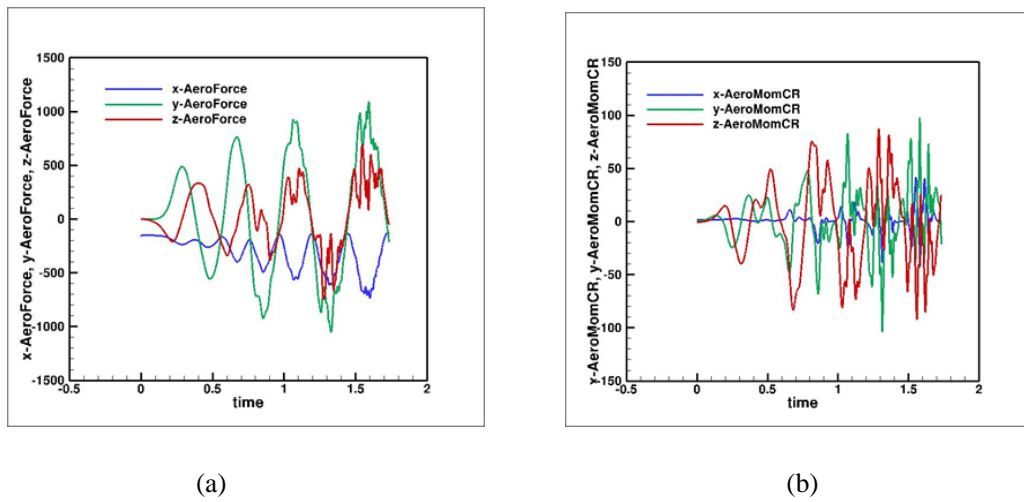


Figure 19. Computed aerodynamics forces (left) and moments (right) as a function of time.

Computed results using coupled CFD/RBD/FCS technique are compared with the results obtained using the standard control design method (BoomFCS) and are shown in Figure 20 through 25. In the standard control design method, the lifting line theory was used to obtain an aerodynamic model for the deflecting canards. As explained earlier, CFD/RBD procedure was used to extract [18] the baseline aerodynamics for the projectile with canards in the undeflected position. In Figures 20-25, coupled CFD/RBD/FCS results are shown in red and the results obtained using the standard control design method are shown in blue. Figures 20(a) and 20(b) show the time histories of the y- and the z-coordinates of the projectile, respectively. As shown in Figure 20(a), initially it takes almost 0.2 sec before the projectile starts moving sideways in the positive y-direction. The oscillations seen in the standard control method is rather small; however, the oscillations seen in the coupled calculation are much larger and seem to also grow with time. Comparison of the z-distances between the two methods shows very similar behavior. The Euler pitch and yaw angle variations are shown in Figure 21. Both methods show similar behavior in the beginning, but with time these angles seem to grow in magnitude with the coupled method whereas they stay almost unchanged in the standard control design method. Figure 22 shows the velocity components (v and w) and Figure 23 shows the comparison of the pitch and the yaw rates. In general, much larger magnitudes are seen in the computed coupled results compared to the standard control design method. Comparisons of the aerodynamic forces, F_y and F_z are shown in Figure 24. Comparison of the aerodynamic force, F_y is good initially up to $t = 0.4$ sec. Later in time the amplitude builds up in the coupled result and much larger forces are observed compared to that used in the standard control design method. The aerodynamic moment components, M_y and M_z are shown in Figure 25a and 25b, respectively. Again, comparison between the two sets of results is good initially (up to $t = 0.3$ sec). Beyond that, the coupled CFD/RBD/FCS calculation indicates a different time-history with much larger amplitudes of oscillations especially in the yawing moment, M_z (Figure 25b).

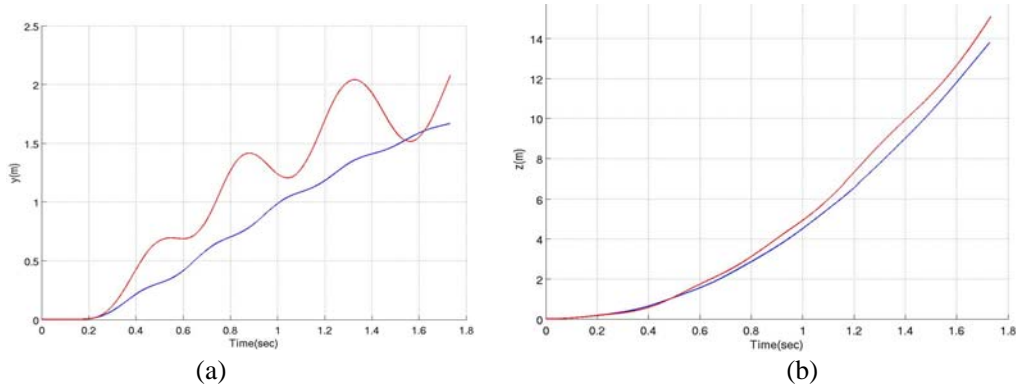


Figure 20. Cross-range distance y (left) and z (right) as a function of time.

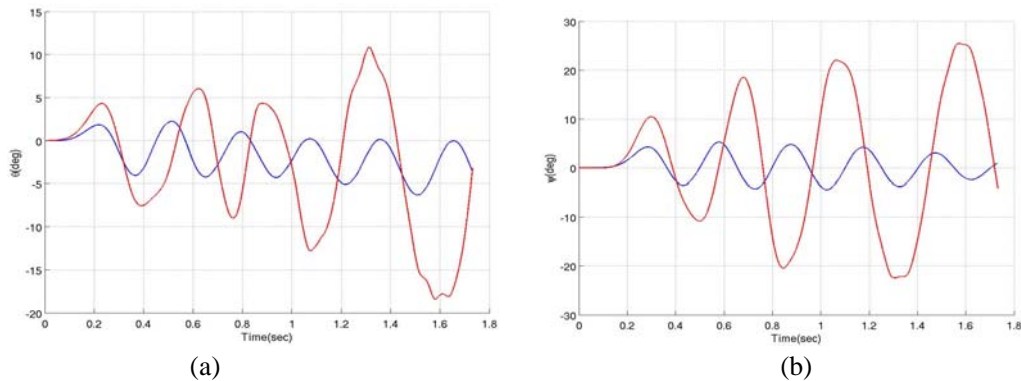


Figure 21. Euler pitch angle (left) and Euler yaw angle (right) as a function of time.

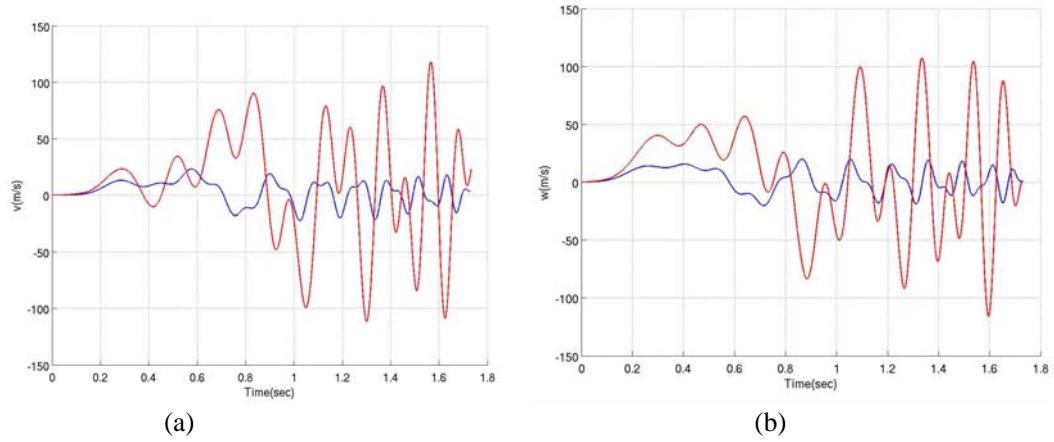


Figure 22. Velocity components as a function of time, (a) v and (b) w .

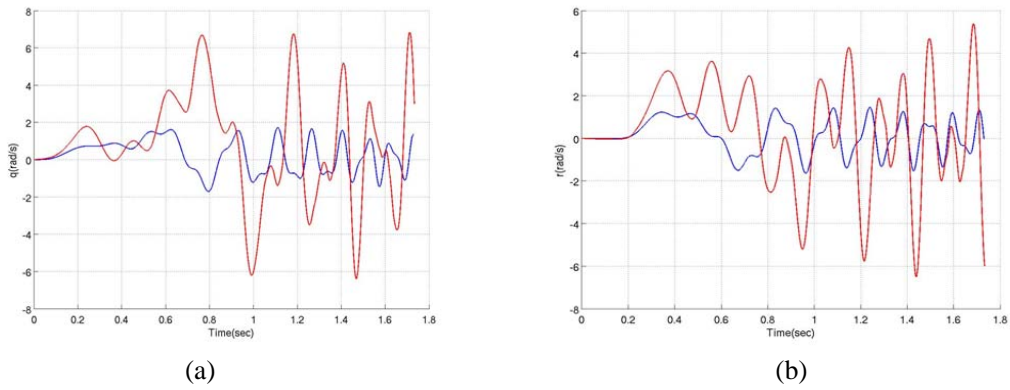


Figure 23. Pitch and yaw rates as a function of time, (a) pitch rate, q and (b) yaw rate, r .

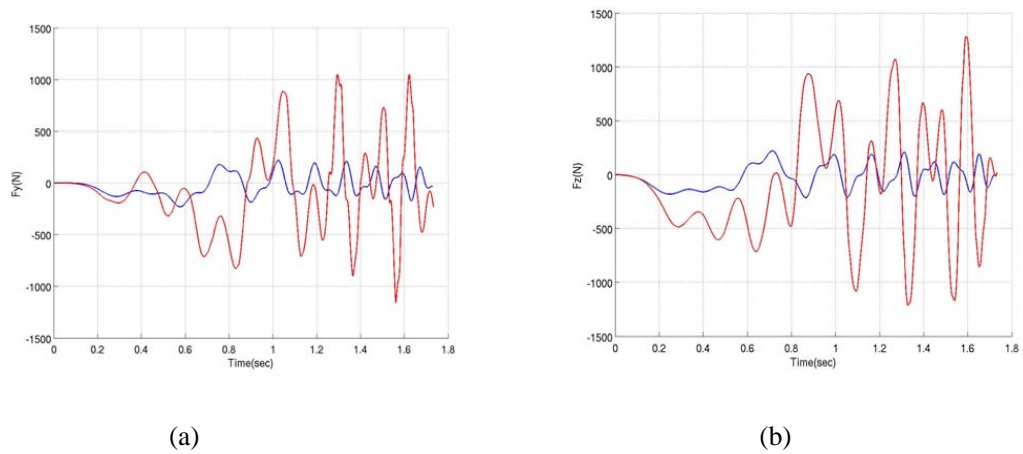


Figure 24. Computed aerodynamics forces as a function of time, (a) F_y , and (b) F_z .

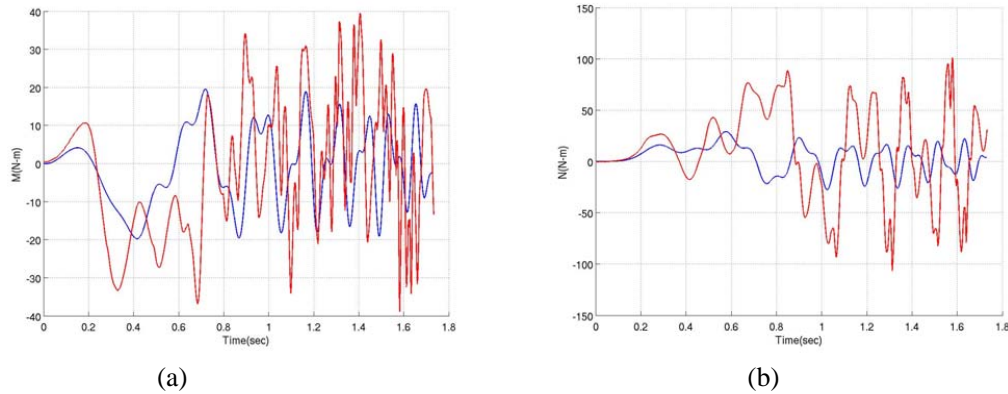


Figure 25. Computed aerodynamics moments as a function of time, (a) M_y , and (b) M_z .

Clearly, the response of the cross-range control maneuver is less than desirable and should be improved. In an attempt to achieve a better response in the cross-range control, several CFD and FCS parameters were varied. Two important CFD parameters, the time-step and inner global iterations used in the dual-time stepping method) were varied. Fifteen inner global iterations were found to be sufficient for good time-accuracy. Results using 15 inner global iterations and different time steps ($2.8877e-04s$, $5.7754e-04s$, and $1.4438e-03s$) produced essentially very similar results. No improvement in the computed coupled results was found by tuning the CFD parameters. In all these cases, the same cross-range controller design was used and the coupled results were based on one cross-range controller design. In order to improve the desired response, one needs to look at FCS parameters or better FCS designs. The FCS design itself requires as best an aerodynamics model as possible. One way to achieve this was to run a coupled CFD/RBD/FCS case and use the coupled results to regenerate a better aerodynamic model of the projectile and use this new aerodynamic model to tune the FCS. A new improved FCS design was thus developed with reduced gain parameters, $K_p = 0.03$ and $K_D = 0.022$ (compared to $K_p = K_D = 0.1$ used in the original FCS design). The FCS design also used $K_I = 0.0006$. A new coupled CFD/RBD/FCS calculation was performed using these parameters in an attempt to obtain a better cross-range control maneuver response.

Figures 26 through 30 show the coupled results obtained using this new (modified) FCS design and are compared with the coupled results obtained with the original FCS design. The angle of attack (α) and the side slip angle can be computed from the computed velocity components u , v , and w and are shown in Figure 26. The α component increases initially from zero about 10° with the original design and about 5° with the modified design in 0.5s of time, goes through zero near $t = 0.75s$, and then start oscillating about zero. Results obtained from both FCS designs show similar behavior in beta component also except it decreases initially with time. For both α and beta components, however, the amplitude of oscillations are generally larger with original design especially after $t = 1.0s$. Coupled results obtained with the modified design become stable with amplitude of oscillation dropping a degree or below whereas the results from the original design clearly show larger angles with no decay.

The total aerodynamic angle of attack, which is the square root of the sum of the squares of the angle of attack components, can then be obtained at each time step as the projectile moves down range. Comparison of the total angle of attack and the motion plot are shown in Figure 27a and Figure 27b, respectively. As seen in Figure 27a, the mean in the total aerodynamic angle of attack keeps increasing in the original FCS design case to a value of about 14° towards the end of the coupled calculation. This increase in the total angle of attack is consistent with the increase in the magnitudes of the aerodynamic forces and moments (see Figure 19). Coupled results obtained with

the modified FCS design show the total angle of attack increasing to about 7.5° in about $t = 0.7s$ and then starts decreasing to 1.3° at $t = 2.5s$. Figure 27b shows a motion plot showing the variation of alpha with beta. The motion plot clearly shows the large angles (nearly $\pm 30^\circ$) associated with the original design and a much better response with the modified design.

Figures 28 and 29 show the time-histories of the computed aerodynamic forces and moments obtained with both the original and the modified FCS designs. These figures clearly show the unsteady nature of the aerodynamic forces and moments during the guided flights. As seen in Figure 28, the amplitudes of oscillations in the aerodynamic force components are seen to increase with time for the original FCS design. As indicated earlier, this is due to an increase in the aerodynamic angle of attack with time for this case. The aerodynamic force components behavior is much better with the modified FCS design and quite opposite to that observed in the original design case. Comparison of the aerodynamic moment components obtained using the two FCS designs are shown in Figure 29. Similar behavior observed in the aerodynamic force components can also be seen in this figure for the aerodynamic moment components. The aerodynamic moment components used in the modified FCS design are well behaved and are much smaller in magnitudes than their counterparts with the original FCS design.

Figure 30 show the variations of the commanded y-distance and the associated canard deflection angle with time for both FCS designs. As seen in Figure 30a, the commanded value in the y-distance is reached a little quicker with the original design compared to the results obtained with the modified design. However, it is oscillatory with the amplitude of oscillation increasing with time and is not desirable. A much smoother response is obtained with the modified FCS design. The commanded value is reached in two seconds, but it seems to overshoot to about 2.5m and is then seen to decrease towards the commanded value of 2m. Comparison of the corresponding canard deflection angles are shown in Figure 30b. As shown in this figure, initially the canard deflection angle is seen to increase with both FCS designs. Later in time however, the canard deflection angle seems to be saturated with the original design. The canard deflection angles are well within the maximum specified angle of 10° and are generally much smaller in magnitudes in the modified design case.

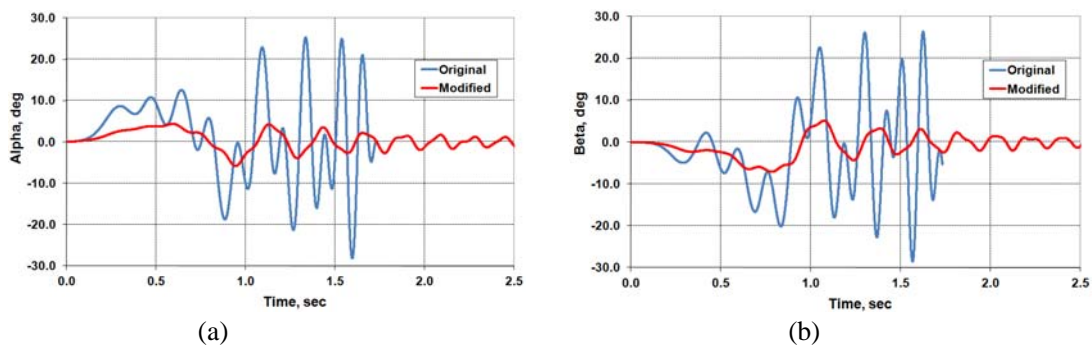


Figure 26. Angle of attack components as a function of time, (a) alpha, (b) beta.

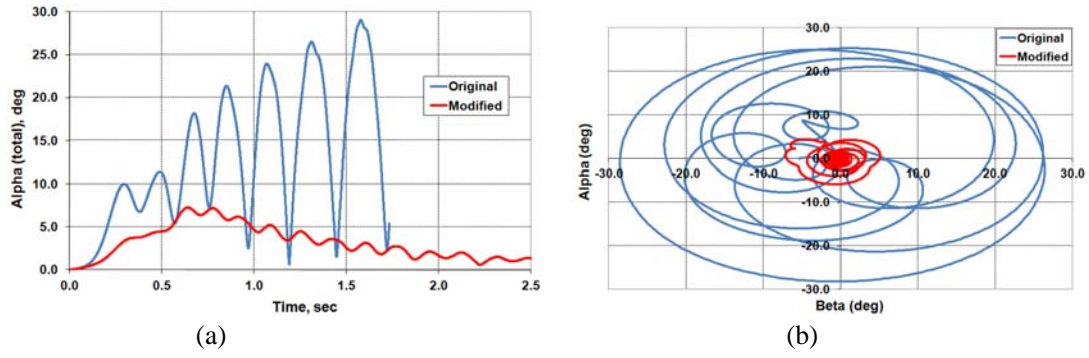


Figure 27. Total angle of attack (a) as a function of time, and motion plot (b).

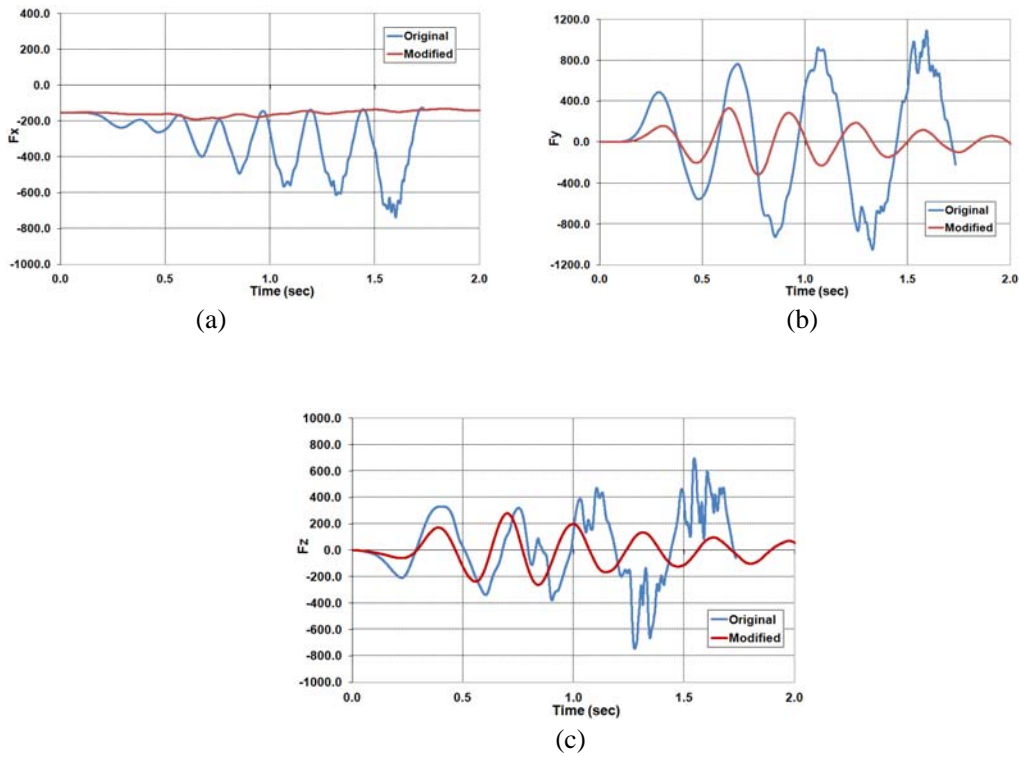
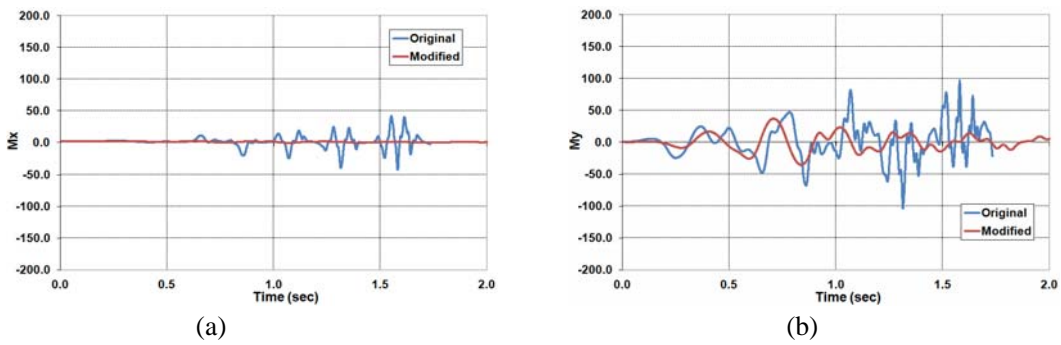
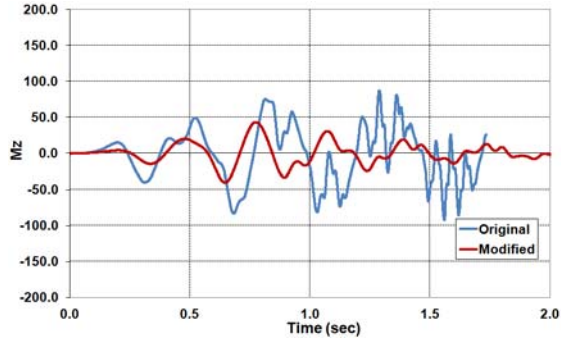


Figure 28. Computed aerodynamics forces as a function of time, (a) F_x , (b) F_y , and (c) F_z .





(c)

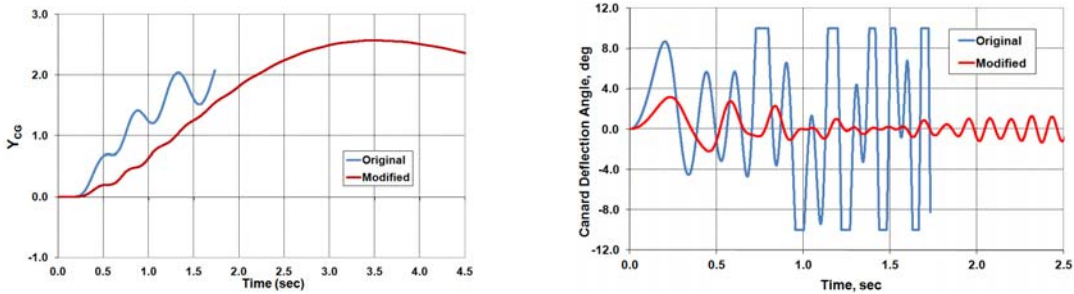
Figure 29. Computed aerodynamics moments as a function of time, (a) M_x , (b) M_y , and (c) M_z .

Figure 30. Computed y-distance (a) and canard deflection angle (b) as a function of time.

It should be noted that in case of the original FCS design, the undesirable time response of the controller was the result of an inadequate aerodynamic model used for the deflecting canards. Without a good aerodynamic model the FCS cannot be successful. The modified FCS design has clearly produced improved results for the cross-range control of the projectile, in large part because it used an improved aerodynamic model for the deflecting canards. Can we improve the FCS design even further? It may be possible to obtain other superior controller designs and improve the command response, but the coupled results shown here do demonstrate the capability of the coupled CFD/RBD/FCS for guided flight of a canard-controlled projectile.

5 Conclusion and Future Work

This paper describes the development and application of an advanced time-accurate coupled CFD/RBD/FCS multidisciplinary technique for prediction of unsteady aerodynamics and flight dynamics of maneuvering projectiles.

A FCS methodology was implemented into a coupled CFD/RBD procedure and a coupled CFD/RBD/FCS capability was developed. The implementation of FCS design into coupled CFD/RBD virtual fly-out simulations is a significant advancement and was demonstrated with a roll control and a cross-range control of a canard-controlled projectile with control law and feedback loop. In the roll control case, coupled CFD/RBD/FCS results clearly show that there is an adverse interaction effect of the canards on the rear fins in a direction opposite to the desired roll. Standard control design method predicts a much different response since it does not take into account this interference effect. In the cross-range control case, the time response was oscillatory and undesirable with the original FCS design because of the inadequacy in the aerodynamic model; however, a much improved response was obtained using a modified FCS design based on an improved aerodynamic model for the deflecting canards.

The effect of canard control maneuvers on the aerodynamics and flight dynamics of canard-controlled projectiles can now be determined using the coupled CFD/RBD/FCS procedure. This coupled procedure can also be extended for simulation of control maneuvers due to jets, flaps, and other flow control mechanisms. Current and future research effort will help determine the potential of these techniques for providing the actual time-dependent response and the resulting unsteady aerodynamics and flight dynamics of maneuvering projectiles for both guided and unguided maneuvers.

Acknowledgements

The authors would like to thank the Department of Defense High Performance Computing Modernization program office for sponsoring this work as a part of a grand challenge project and for providing critically needed HPC resources at the Air Force Research Laboratory Supercomputing Resource Center for successful accomplishment of the work. The authors also wish to thank Dr. Sukumar Chakravarthy of the Metacomp Technologies for his technical assistance in the development of coupled CFD/RBD/FCS procedure.

References

- [1] S. Silton. Navier-Stokes Computations for a Spinning Projectile from Subsonic to Supersonic Speeds. *Journal of Spacecraft and Rockets*, Vol 42, No 2, pp 223-231, 2005.
- [2] J. Sahu. Virtual Fly-Out Simulations of a Spinning Projectile from Subsonic to Supersonic Speeds. AIAA Applied Aerodynamics Meeting, Honolulu, HI, June 2011.
- [3] J. Sahu, K. R. Heavey, and E. N. Ferry. Computational Fluid Dynamics for Multiple Projectile Configurations. Proceedings of the 3rd Overset Composite Grid and Solution Technology Symposium, Los Alamos, NM, October 1996.
- [4] J. Sahu, J. Despirito, H. Edge, S. Silton, and K. Heavey. Recent Applications of Structured and Unstructured Grid Techniques to Complex Projectile and Guided Missile Configuration. Proceedings of the Eighth International Grid Generation and Computational Field Simulations Conference, Honolulu, HI June 2002.
- [5] J. DeSpirito, and P. Plostins. CFD Prediction of M910 Projectile Aerodynamics: Unsteady Wake Effect on Magnus Moment. AIAA-2007-6580, Aug. 2007.
- [6] J. Sahu. Time-Accurate Numerical Prediction of Free Flight Aerodynamics of a Finned Projectile. ARL-TR-3603, Aberdeen Proving Ground, MD, September 2005.
- [7] J. Sahu. Time-Accurate Computations of Free-Flight Aerodynamics of a Spinning Projectile With and Without Flow Control. ARL-TR-3919, Aberdeen Proving Ground, MD, September 2006.
- [8] J. Sahu and K.R. Heavey. Time-Accurate Computations for Rapid Generation of Missile Aerodynamics. AIAA Atmospheric Flight Mechanics Meeting, Toronto, Canada, 2-6 August 2010.
- [9] J. Sahu. Unsteady CFD Modeling of Aerodynamic Flow Control over a Spinning Body with Synthetic Jet. AIAA Paper 2004-0747, Reno, NV, 5-8 January 2004.
- [10] J. Sahu. Time-Accurate Numerical Prediction of Free-Flight Aerodynamics of a Finned Projectile. *AIAA Journal of Spacecraft and Rockets*, Vol. 45, No 5, pp 946-954, 2008.
- [11] M. Costello. Extended Range of a Gun Launched Smart Projectile Using Controllable Canards. *Shock and Vibration*, Vol 8, No 3-4, pp 203-213, 2001.
- [12] T.H. Pulliam, and J. L. Steger. On Implicit Finite-Difference Simulations of Three-Dimensional Flow. *AIAA Journal*, vol. 18, no. 2, pp. 159-167, February 1982.
- [13] O. Peroomian, S. Chakravarthy, and U. Goldberg. A 'Grid-Transparent' Methodology for CFD. AIAA Paper 97-07245, 1997.
- [14] O. Peroomian, S. Chakravarthy, S. Palaniswamy, and U. Goldberg. Convergence Acceleration for Unified-Grid Formulation Using Preconditioned Implicit Relaxation. AIAA Paper 98-0116, 1998.

- [15] U.C. Goldberg, O. Perroomian, and S. Chakravarthy. A Wall-Distance-Free K-E Model With Enhanced Near-Wall Treatment. *ASME Journal of Fluids Engineering*, Vol. 120, pp. 457-462, 1998.
- [16] Metacomp Technologies, Inc. MIME Software, Agoura Hills, CA.
- [17] J. Sahu and C. J. Nietubicz. Application of Chimera Technique to Projectiles in Relative Motion. *AIAA Journal of Spacecraft & Rockets*, Sept-Oct 1995.
- [18] M. Costello, and C. Montalvo. Estimation of Projectile Aerodynamic Coefficients Using Coupled CFD/RBD Simulation Results. *AIAA Atmospheric Flight Mechanics Conference*, Toronto, Canada, 2010.